JOURNAL OF GEOPHYSICAL RESEARCH, VOL. 96, NO. B9, PAGES 14,319–14,330, AUGUST 10, 1991

The Shock Wave Equation of State of Brucite $Mg(OH)_2$

THOMAS S. DUFFY AND THOMAS J. AHRENS

Seismological Laboratory, California Institute of Technology, Pasadena

MANFRED A. LANGE

Alfred Wegner Institute for Polar and Marine Research, Bremerhaven, Germany

New equation of state (EOS) data for brucite $Mg(OH)_2$ shocked between 12 and 60 GPa are reported. When combined with earlier data of Simakov et al. (1974), it is found that brucite EOS data between 12 and 97 GPa can be fit with a single linear U_s-u_p relationship: $U_s = 4.76(0.11) + 1.35(0.05)u_p$. The third order Birch-Murnaghan equation parameters are: $K_{os} = 51 \pm 4$ GPa and $K'_{os} = 5.0 \pm 0.4$. The lack of a U_s-u_p discontinuity indicates that no phase transformation with a significant volume change occurs to at least 97 GPa. However, thermodynamic and theoretical Hugoniot calculations suggest brucite may dehydrate with only a small volume change. A lower bound for this dehydration pressure under shock conditions is inferred to be 26 GPa. We report the first partial release states measured for this material. The data are in quantitative agreement with earlier shock recovery experiments (Lange and Ahrens, 1984). Volatilization upon release begins at pressures as low as 12 GPa, much less than predicted by the shock entropy method. Calculated phase boundaries using the present EOS data are consistent with experimental data and indicate that brucite is unlikely to be stable under lower mantle conditions. However, brucite data, in conjunction with data for silicates and oxides, can be used to infer the effect of H_2O on lower mantle properties. At high pressure, bulk sound velocities calculated for MgO and $Mg(OH)_2$ are very similar, indicating that the presence of hydrous assemblages in the lower mantle may not produce anomalous bulk seismic velocities. Comparison of densities in brucite and other high-pressure phases under mantle conditions indicates that the water content of the lower mantle is between 0 and 3 wt %.

INTRODUCTION

For more than 20 years, shock wave data have played an important role in studying both the accretion of the Earth and the composition of the interior. Volatilization of impacting planetesimals has been shown to be an important process in the evolution of the Earth's atmosphere [*Ahrens*, 1990]. It may also have a profound effect on the evolution of the interior since thermal blanketing by a thick early atmosphere could have resulted in extensive melting of the Earth [*Abe and Matsui*, 1986]. The stability of hydrous minerals under mantle conditions is also an important consideration in atmospheric evolution as degassing of the mantle over geologic time can also possibly explain the present atmosphere, particularly if any primitive atmosphere was stripped by impact of a moon-forming bolide.

During accretion, some fraction of the incoming volatile budget is incorporated into the growing planet. The incorporation and retention of water would have large dynamical and structural effects. The presence of free water in the upper mantle has been proposed as an explanation for the seismic low velocity zone [*Liu*, 1989]. Reactions involving water-bearing minerals may play a role in generating deep subduction zone earthquakes [*Meade and Jeanloz*, 1989]. The presence of a few wt. % water could alter mantle mineralogy [*Liu*, 1987]. The effect of water on mantle dynamics has also been recently studied. The presence of water would reduce mantle viscosity and result in lower mantle temperatures for a given thermal output [*McGovern and Schubert*, 1989]. Water would lower the mantle solidus as well, possibly allowing small amounts of hydrous partial melts to exist in the lower mantle [*Duffy and Ahrens*, 1990*a*].

In this paper, the behavior of the hydrous mineral brucite, $Mg(OH)_2$, is studied under shock loading conditions. The results are brought to bear on both the volatilization of incoming material and the role of water in the Earth's interior. Brucite is an ideal material to study in these respects since it is water-rich (25-30 wt. % H_2O) and because it is structurally and compositionally simple. Our results complement a recent shock wave study of the hydrous silicate serpentine [*Tyburczy et al.*, 1991].

Previously, *Simakov et al.* [1974] acquired shock data on brucite to 97 GPa. Their results provided no clear evidence for dehydration or other phase changes. We wished to reexamine this result and its potential implications for the Earth's interior. In addition, we report the first measurements of isentropic release states in brucite. These results are then compared to shock recovery data [*Lange and Ahrens*, 1984] and theoretical predictions of volatilization and applied to Earth accretion models.

EXPERIMENTAL DETAILS

The natural brucite samples used in this study originated from Lodi, Nevada and Texas, Pennsylvania. Bulk chemical analyses of representative samples are shown in Table 1. The average Archimedean bulk density of the samples was 2.382 ± 0.022 g/cm^3. The average crystal density, determined by weighing the samples in air and toluene under controlled temperature conditions, was 2.391 ± 0.017 g/cm^3. This agrees well with the tabulated density of 2.39 g/cm^3 [*Hurlbutt and Klein*, 1977]. The porosity of the samples was

Paper number 91JB00987.
0148-0227/91/91JB-00987$05.00

TABLE 1. Chemical Composition of Brucite Samples

Oxide	Wt. %
MgO	76.122
FeO	0.393
SiO_2	0.184
MnO	0.015
Cr_2O_3	0.007
Na_2O	0.003
CaO	0.003
TiO_2	0.002
Al_2O_3	0.000
H_2O	25.394
Total	102.123

Average of seven analyses of brucite from Texas, Pennsylvania. H_2O obtained by thermogravimetric analysis. Others obtained by electron microprobe; all Fe reported as FeO.

exceptionally small as the average difference between the bulk and crystal density was 0.4%. All samples were machined into rectangular targets 3-3.5 mm thick with lateral dimensions at least 10 mm.

Subsequent chemical analysis revealed that some samples from Lodi, Nevada contained potentially significant amounts of calcium hydroxide (portlandite). By comparing measured crystal densities with those expected for brucite and portlandite [*Roberts et al.*, 1990], we find that samples used in shots 200, 742, 744, and 745 may have contained more than 10 mol.% portlandite. Shots 744 and 745 may contain the most calcium hydroxide with maximum amounts of 24% and 44%, respectively. The implications of this sample variability will be discussed in a later section.

Shock compression of brucite was achieved using the Caltech 40-mm propellant and 25-mm light gas guns which together are capable of launching metallic flyer plates between 0.8 and 6.5 km/s. Projectile velocity was determined both by double exposure flash X ray photography and by laser interruption intervals on the 40-mm gun. On the light gas gun, projectile velocity was measured using two 15-ns flash X ray sources and electronic time interval counters. Targets consisted of a metallic driver, brucite sample, and a low density buffer material. The targets were stepped so that two small mirrors could be epoxied onto the rear surface of the driver and sample. An additional mirror was affixed to the rear surface of the buffer. Shock wave velocities in the target and buffer were determined by recording the destruction of the mirrors by the shock arrival via an image converter streak camera and Xenon light source. More detailed discussions of the experimental technique may be found in *Jackson and Ahrens* [1979] and *Ahrens* [1987].

Tungsten and aluminum flyer and driver plates were used, with symmetric impact conditions applying in all experiments. Equation of state (EOS) parameters for the flyers and drivers are listed in Table 2. Material velocity behind the shock front was determined through impedance matching [*Ahrens*, 1987] and pressure-volume states were calculated using the Rankine-Hugoniot equations which relate thermodynamic variables to the kinematic variables of the flow. Uncertainties were determined by standard error propagation techniques [*Jackson and Ahrens*, 1979].

TABLE 2. Equation of State Standards

Material	u_p Range, km/s	ρ_o, g/cm^3	c_o, km/s	s
Tungsten	0-2.1	19.24	4.04	1.23
Aluminum 1100	0-1.8	2.71	5.38	1.34
Polystyrene foam	0-4.8	0.0497	0.243	1.118
	5.6-7.9	0.0497	-0.493	1.354
Lexan	0-2.9	1.196	2.449	1.498
Graphite foam	0-4.7	1.011	0.79	1.30

All data from *Marsh* [1980].

Partial release states were obtained by measuring the shock wave transit time through low impedance buffers in contact with the sample. The buffer materials were lexan, polystyrene foam, and graphite foam (Table 2). The pressure and particle velocity at the buffer-sample interface were determined from the measured shock velocity and the known buffer equation of state. An upper bound for the density of the partially released state is obtained by integrating the Riemann integral over a linear P-V path [*Lyzenga and Ahrens*, 1978].

RESULTS AND DISCUSSION

A total of 13 Hugoniot equation of state experiments were conducted on brucite specimens. Peak shock pressures ranged between 12 and 60 GPa. The experimental parameters are listed in Table 3, while the results of shock and release experiments are shown in Tables 3 and 4. The results of those shots potentially containing significant amounts of Ca are largely indistinguishable from the others, and consequently, all will be considered together. The small amount of scatter in the data indicates that sample variability is not a significant problem in these experiments. The results of shot 200, however, lie significantly outside the uncertainty range of the remainder of the data and will be excluded from subsequent analysis. The exceptionally high density resulting from this shot may be due to transformation of the Ca-rich component to a high-pressure phase as expected from static compression studies [*Meade and Jeanloz*, 1990].

Compression States

In Figure 1, new shock compression data for brucite are presented in the shock velocity-particle velocity plane along with the earlier data of *Simakov et al.* [1974]. The present data appear to be slightly more incompressible, however, the two data sets are consistent in that there is no measurable change in slope throughout the pressure range of the data. This indicates that no phase transition with an appreciable volume change is occurring within the pressure and temperature range of these experiments. The density reported by *Simakov et al.* [1974] is 2.37 g/cm^3, which is 0.5% less then the average of our samples. Thus, the samples of Simakov et al. may have more porosity, water, or light impurities.

It is known empirically that shock wave data for many materials can be described by a linear function of the form:

$$U_s = c_o + su_p \quad (1)$$

where U_s is the shock wave velocity, u_p is the material velocity behind the shock, c_o is the zero pressure bulk sound ve-

TABLE 3. Brucite Hugoniot Experiments

Shot	Flyer/ Driver	u_{fp}, km/s	ρ_o, g/cm^3	U_s, km/s	u_p, km/s	P, GPa	ρ, g/cm^3
553	W	2.419	2.397	7.489	2.007	36.02	3.275
		0.031	0.003	0.051	0.026	0.52	0.019
554	W	2.343	2.387	7.526	1.941	35.01	3.230
		0.099	0.003	0.080	0.084	1.54	0.050
670	W	1.873	2.400	6.916	1.567	26.00	3.103
		0.030	0.001	0.067	0.026	0.47	0.018
671	W	1.551	2.388	6.603	1.305	20.57	2.975
		0.016	0.001	0.066	0.014	0.28	0.011
742	W	2.360	2.377	7.457	1.961	34.76	3.225
		0.026	0.002	0.049	0.022	0.44	0.016
743	W	2.433	2.382	7.523	2.019	36.19	3.256
		0.033	0.001	0.023	0.028	0.51	0.017
744	W	1.894	2.360	6.924	1.588	25.96	3.062
		0.034	0.002	0.131	0.029	0.63	0.026
745	W	1.891	2.325	7.004	1.587	25.83	3.007
		0.030	0.033	0.105	0.026	0.62	0.048
750	W	1.508	2.393	6.557	1.269	19.91	2.967
		0.015	0.002	0.055	0.013	0.25	0.010
751	W	1.017	2.410	5.870	0.886	12.25	2.827
		0.011	0.004	0.128	0.010	0.27	0.014
199	Al	4.699	2.384	8.387	2.494	49.86	3.393
		0.004	0.001	0.201	0.028	0.78	0.049
200	Al	5.602	2.378	8.185	3.079	59.94	3.812
		0.003	0.003	0.164	0.029	0.84	0.065
208	Al	5.194	2.394	8.686	2.753	57.26	3.505
		0.006	0.002	0.283	0.039	1.19	0.075

W, tungsten; Al, aluminum 1100; u_{fp}, flyer plate velocity; and ρ_o, initial bulk density.

locity, and the parameter s is related to the pressure derivative of the zero pressure bulk modulus K'_{os} by

$$K'_{os} = 4s - 1 \tag{2}$$

This is known as the shock wave equation of state.

A linear weighted least squares fit to the data of Table 1 yields

$$U_s = 4.83(0.10) + 1.34(0.05)u_p$$

where the numbers in parentheses represent one standard deviation uncertainties. *Simakov et al.* [1974] did not report uncertainties for their experiments. An unweighted least squares fit to their data yields

$$U_s = 4.46(0.22) + 1.41(0.08)u_p$$

The two data sets overlap at the 2σ level. We therefore adopt the combined data set as representing the shock wave equation of state of brucite. A least squares fit to all the data using equal weights gives

$$U_s = 4.76(0.11) + 1.35(0.05)u_p$$

which is similar to the fit from the present data alone. The zero pressure bulk modulus from the shock wave EOS is 54 $\pm$ 3 GPa and the first pressure derivative is 4.4 $\pm$ 0.2.

Zero pressure sound velocities were measured ultrasonically for several samples. Average compressional and shear velocities were 6.28(0.18) km/s and 2.95(0.19) km/s, yielding a bulk sound velocity of 5.28(0.26) km/s which is about 10% greater than the U_s-u_p intercept, c_o, obtained from our experiments.

Pressure-density states attained in the shock compression of brucite are shown in Figure 2. The results may be better understood by reducing the data to an isentrope and fitting to a Birch-Murnaghan EOS. A convenient formalism for achieving this is the normalized pressure-normalized strain or F-f formalism [*Birch*, 1978] adapted for Hugoniot analysis [*Heinz and Jeanloz*, 1984; *Ahrens and Jeanloz*, 1987].

The Eulerian strain, f, is expressed as

$$f = \frac{1}{2}\left[\left(\frac{\rho}{\rho_o}\right)^{\frac{2}{3}} - 1\right] \tag{3}$$

where ρ and ρ_o are Hugoniot and ambient densities respectively. The normalized pressure, F, reduced from Hugoniot to isentropic conditions is

$$F = \frac{1 - \frac{\gamma}{2}\left[(1+2f)^{\frac{3}{2}} - 1\right]}{3f(1+2f)^{\frac{3}{2}}\left[1 + (2 - 1.5\gamma)f\right]}P \tag{4}$$

where γ is the Gruneisen parameter and P is the Hugoniot pressure. The Birch-Murnaghan equation to third order in strain can be expressed as a linear equation:

TABLE 4. Brucite Partial Release States

		Measured				Calculated	
Shot	Buffer	U_{sb}, km/s	u_{pb}, km/s	P_b, GPa	ρ_b, g/cm^3	ρ_c, g/cm^3	T_c, K
553	Lexan	6.551	2.738	21.40	2.924	3.009	737
		0.194	0.130	1.65	0.153		
	Polystyrene	4.615	3.911	0.90	2.448	2.414	678
		0.079	0.071	0.03	0.058		
554	Lexan	6.381	2.625	19.98	2.935	2.968	715
		0.194	0.130	1.59	0.185		
	Graphite	4.897	3.159	16.54	2.565	2.889	708
		0.070	0.054	0.52	0.158		
670	Lexan	5.662	2.145	14.49	2.847	2.860	531
		0.081	0.054	0.57	0.070		
	Polystyrene	4.630	3.924	0.90	1.840	2.427	498
		0.094	0.084	0.04	0.064		
671	Lexan	5.230	1.856	11.58	2.703	2.775	445
		0.129	0.086	0.82	0.103		
	Polystyrene	3.771	3.156	0.59	1.970	2.406	420
		0.089	0.080	0.03	0.062		
742	Lexan	6.459	2.677	20.63	2.887	2.973	710
		0.166	0.111	1.38	0.129		
	Polystyrene	5.571	4.766	1.32	1.834	2.412	655
		0.085	0.076	0.04	0.051		
743	Lexan	6.513	2.713	21.08	2.950	3.041	746
		0.103	0.069	0.87	0.084		
	Graphite	4.815	3.096	15.94	2.745	2.923	736
		0.060	0.046	0.44	0.064		
744	Lexan	5.743	2.199	15.07	2.722	2.833	530
		0.089	0.059	0.64	0.084		
	Polystyrene	4.665	3.955	0.92	1.817	2.388	496
		0.099	0.089	0.04	0.068		
745	Lexan	5.700	2.170	14.76	2.752	2.824	531
		0.088	0.059	0.63	0.083		
	Graphite	4.084	2.534	10.46	2.558	2.711	523
		0.077	0.059	0.44	0.081		
750	Polystyrene	3.659	3.055	0.56	1.993	2.410	412
		0.066	0.059	0.02	0.048		
751	Lexan	4.294	1.232	6.31	2.658	2.645	348
		0.199	0.133	0.97	0.143		
	Polystyrene	2.509	2.027	0.25	2.146	2.419	336
		0.031	0.028	0.01	0.031		
199	Polystyrene	6.821	5.402	1.83	2.124	2.429	1143
		0.199	0.147	0.10	0.086		
200	Graphite	6.245	4.196	26.49	3.338	3.088	1373
		0.226	0.174	2.06	0.167		
208	Polystyrene	8.959	6.981	3.11	1.625	2.468	1213
		0.324	0.239	0.22	0.104		

U_{sb}, buffer shock velocity; u_{pb}, release state particle velocity; P_b, release state pressure; ρ_b, release state density of brucite; ρ_c, calculated release state density using (17) and (18); T_c, calculated release state temperature using (19).

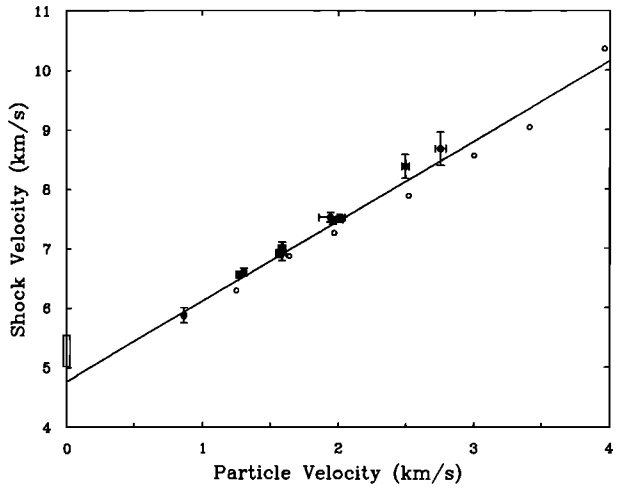

Fig. 1. Shock velocity-particle velocity data for brucite. Solid circles with error bars are data from this study (Table 2). Open symbols are data reported by *Simakov et al.* [1974]. The line is a least squares fit to the combined data set. The range of ultrasonically determined bulk sound velocities is shown by the box along the y axis.

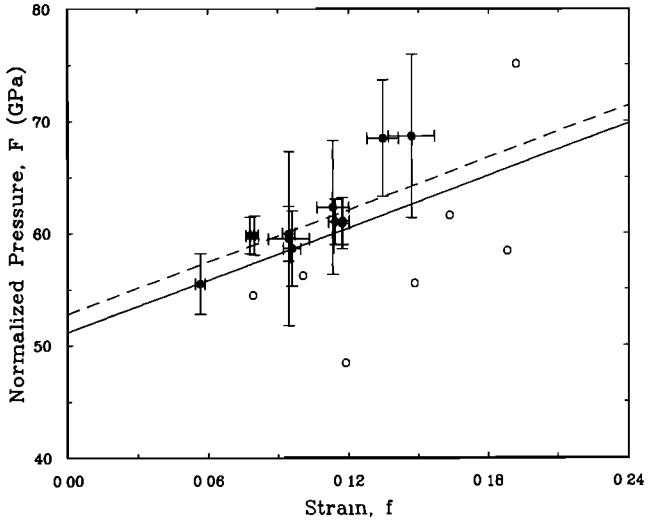

Fig. 3. Shock data for brucite in the normalized pressure (F)-normalized strain (f) representation. Symbols are the same as in Figures 1 and 2. The solid curve is a straight line fit to the combined data set with all data weighted equally. The dashed curve is a weighted fit to the present data only (solid symbols) .

$$F = K_{os}(1 - 2\xi f_{3H}) \tag{5}$$

where K_{os} is the 0 pressure isentropic bulk modulus and f_{3H} is given by

$$f_{3H} = \frac{f[1 + (2 - \gamma)f]}{1 + (2 - 1.5\gamma)f} \tag{6}$$

and

$$\xi = \frac{3}{4}(4 - K'_{os}) \tag{7}$$

The data are presented in the F-f plane in Figure 3.

One source of uncertainty in this calculation is the Gruneisen parameter, γ. Its value can be obtained from the thermodynamic identity

$$\gamma_o = \frac{\alpha K_{os}}{\rho_o C_p} \tag{8}$$

The volume coefficient of thermal expansion, α, of brucite is unknown, but we estimate $\alpha \approx 25 \times 10^{-6} K^{-1}$ based on data for hornblende and MgO [*Skinner*, 1966; *Suzuki*, 1975]. C_p, the specific heat at constant pressure, is 1.325 J/gK for brucite [*Robie et al.*, 1978]. Combining these with ρ_o and K_{os} from above, we estimate that

$$\gamma_o \approx 0.43 \pm 0.40.$$

The volume dependence of γ was modeled by

$$\gamma = \gamma_o \left(\frac{\rho_0}{\rho}\right)^q \tag{9}$$

Values of q between 0 and 2 were considered in the analysis. A linear unweighted least squares fit using (5) to the combined data set yields the parameters: $K_{os} = 51 \pm 4$ GPa and $K'_{os} = 5.0 \pm 0.4$. A weighted least squares fit to the present data alone gives a similar result: $K_{os} = 53 \pm 3$ GPa and $K'_{os} = 5.0 \pm 0.4$. The fit to the combined data in the P-ρ plane is shown in Figure 2. By optimizing phase equilibria and heat capacity data for brucite, *Saxena* [1989] obtained comparable values for the isothermal bulk modulus and pressure derivative: $K_{oT} = 57.1$ GPa and $K'_{oT} = 4.7$.

Jeanloz [1989] has derived a criterion for the formal equivalence of the Birch-Murnaghan and shock wave equations of state. The relation that must be satisfied is $18s\gamma_o = 162s^2 - 360s + 215$. Using the shock wave EOS above, we must have $\gamma_o = 1.0 \pm 0.1$ for this material. This result does not overlap the range of Gruneisen parameters determined from the thermodynamic data above. Thus, the shock wave equation of state and the third order Birch-Murnaghan equation cannot by considered equivalent descriptions for this material. A similar result has been found for serpentine [*Tyburczy et al.*, 1991].

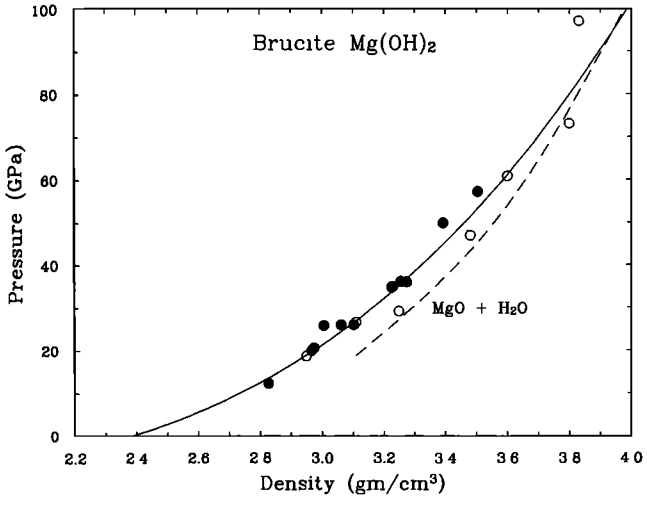

Fig. 2. Pressure-density data for brucite. Solid symbols are data of this study (Table 2). Open symbols are data of *Simakov et al.* [1974]. The dashed curve is a theoretical Hugoniot constructed for an ideal mixture of MgO and H_2O with the thermal corrections described in the text. The solid curve is a fit to the combined data using the normalized pressure-normalized strain formalism (see Figure 3).

An interesting feature of the data is that all the brucite $U_s - u_p$ data can be fit with a single straight line (Figure 1). Most minerals studied to date exhibit slope discontinuities in the $U_s - u_p$ plane which are interpreted as being due to polymorphic phase transitions. Brucite thus joins a small group of minerals (e.g., MgO and Al_2O_3) that can be expressed by a single $U_s - u_p$ relationship to pressures up to at least 97 GPa. However, some phase transitions (e.g., melting) have volume changes that are too small to be detected on the Hugoniot. Any phase transition involving brucite must therefore involve only a small volume change.

Temperatures along the Hugoniot were calculated from the Hugoniot energy equation and the first law of thermodynamics using the method of *McQueen et al.* [1967]:

$$\frac{dT}{dV} = -T\left(\frac{\gamma}{V}\right) + \frac{\frac{dP}{dV}(V_o - V) + P}{2C_v} \quad (10)$$

where T is the temperature, P is the pressure, and V is the specific volume along the Hugoniot. C_v, the specific heat at constant volume, is assumed to be constant with pressure and equal to C_p. The entropy, S, along the Hugoniot can be determined from a similar equation:

$$\frac{dS}{dV} = \frac{\frac{dP}{dV}(V_o - V) + P}{2T} \quad (11)$$

Equations (10) and (11) were integrated numerically using q=1 in (9). The calculated pressure-temperature Hugoniot path is shown in Figure 4.

The equilibrium phase boundary for the reaction

$$Mg(OH)_2 \rightleftharpoons MgO + H_2O \quad (12)$$

was calculated using available data for brucite, periclase, and H_2O. Thermodynamic properties of H_2O were taken from the corresponding state formulation of the virial equation given by *Saxena and Fei* [1987]. The Gibbs free energies obtained from this expression are in agreement with the data of *Halbach and Chatterjee* [1982], who used a modified Redlich-Kwong equation to obtain thermodynamic properties of H_2O to 20 GPa and 1000 °C. Thermodynamic properties of the solid phases were taken from *Robie et al.* [1978]. The properties of brucite above 600 °C were extrapolated using lower temperature data.

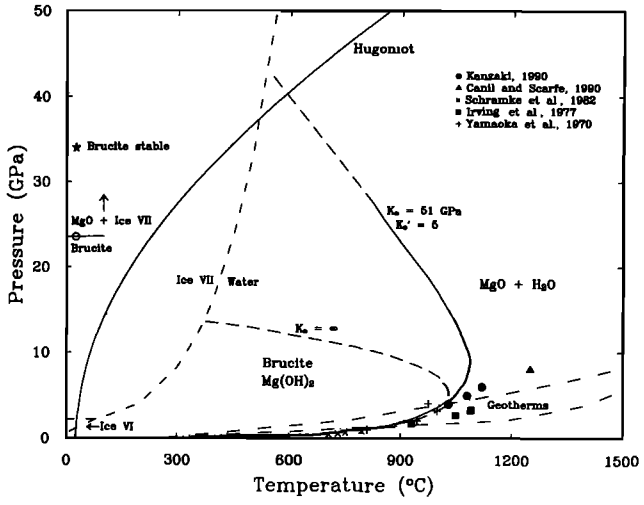

Fig. 4. Calculated phase diagram for brucite. The dashed curve is the boundary for the reaction of (12) when compressibility and thermal expansivity of the solids are not accounted for. The solid curve (dashed above 27 GPa) shows the calculated phase boundary when these factors are included. The solid curve labeled Hugoniot is the shock pressure-temperature path. The dash-dot line is the projected ice VII melting curve [*Mishima and Endo*, 1978]. The open circle represents the lower bound of the calculated dehydration boundary at room temperature. Other symbols represent experimental determinations of brucite-periclase equilibrium. The room temperature vibrational datum of *Kruger et al.* [1989] is represented by the star at 34 GPa. The dash-double dot curves are representative mantle geotherms.

The stability of brucite as a function of pressure and temperature was evaluated using

$$\Delta G_r(P,T) = \Delta G_r(1,T) + \int_1^P \Delta V_s dP + RT \ln f_{H_2O} \quad (13)$$

where ΔG_r is the difference in Gibbs free energy between products and reactants, ΔV_s is the volume change between the solid phases, and f_{H_2O} is the fugacity of water. The dashed curve in Figure 4 shows the phase boundary resulting from the above equation when the effects of compressibility and thermal expansion in the solid phases are neglected. The calculation is in good agreement with experimental data up to 1000 °C. The U-shaped dehydration curve is due to the large compressibility of water. While temperature maxima associated with transformation to dense phases have been observed experimentally for many hydrous minerals, no temperature maximum solely due to H_2O compressibility has been experimentally observed. *Yamaoka et al.* [1970] reported a temperature maximum in the stability of brucite at 1000 °C on the basis of quenched samples. Later work, including DTA results, demonstrates that no temperature maximum occurs to at least 8 GPa and 1250 °C [*Irving et al.*, 1977; *Kanzaki*, 1990; *Canil and Scarfe*, 1990].

The incorporation of thermal expansivity and compressibility of the solid phases has a dramatic effect on the location of the high pressure phase boundary. This is indicated by the solid curve (dashed above 27 GPa) in Figure 4. Thermal expansion and EOS data for periclase were taken from *Suzuki* [1975] and *Jackson and Niesler* [1982]. EOS data for brucite were taken from the present study and the thermal expansion of brucite was assumed to be the same as MgO. High temperature volumes were calculated from

$$V(T) = V_0 \exp\left(\int_{298}^{T} \alpha(T)\, dT\right) \quad (14)$$

where α is the thermal expansion coefficient. The integral in (13) was evaluated using the Murnaghan equation:

$$V(P,T) = V(T)\left(1 + \frac{K_o' P}{K_o}\right)^{-1/K_o'} \quad (15)$$

The stability field of brucite is markedly extended at high pressure because brucite is significantly more compressible than MgO. While this phase boundary is uncertain above 1000 °C, it appears to be in better agreement with the experimental data of *Kanzaki* [1990]. It is also consistent with vibrational spectra indicating that brucite is stable at room temperature to at least 34 GPa [*Kruger et al.*, 1989]. To investigate the stability of brucite at room temperature, we evaluated (13) by directly integrating the compression curve of ice VII [*Hemley et al.*, 1987]. The Gibbs free energy of ice VII at room pressure and temperature must be greater than that of liquid water. The value for water provides a lower bound for the reaction which is calculated to be 24 GPa (Figure 4). This boundary is very sensitive to EOS

parameters of brucite as well as the reference free energy value.

The possibility must also be considered that the EOS parameters of brucite obtained here are biased due to the dehydration reaction. As K_o and K_o' are increased, the calculated stability field of brucite contracts. The phase boundary calculated when compressibility is ignored corresponds to infinite K_o or K_o'. Incorporation of a temperature dependent bulk modulus would expand the brucite stability field, however. The phase diagram based on our EOS is generally consistent with both the high temperature dehydration experiments and the high pressure vibrational data and therefore we believe it provides the best estimate of the stability of brucite available with existing data.

Th extension of the calculated dehydration boundary intersects the brucite Hugoniot at 41 GPa. The equilibrium phase boundary provides a lower bound on the shock dehydration pressure as many reactions need to be strongly overdriven before occurring under shock conditions. The release data discussed below also provide a constraint as we infer that some H_2O is retained upon release from pressures as high as 56 GPa, although most H_2O is lost upon release at 26 GPa. Thus, the release data suggest 26 GPa as a lower bound for the dehydration of brucite under shock conditions.

With available EOS data, a theoretical Hugoniot for the mixed oxide assemblage $H_2O + MgO$ was constructed. Following *Al'tshuler and Sharipdzhanov* [1971], we assume ideal mixing between the oxide phases. The density of the shock compressed mixture is found by averaging the component densities according to their weight fractions:

$$\rho_m(P) = \left[\sum \frac{X_i}{\rho_i(P)}\right]^{-1} \quad (16)$$

where $\rho_m(P)$ is the density of the mixture at Hugoniot pressure P, ρ_i is the density of the oxide component, and X_i is the weight fraction of the component. This method has been shown to be successful in predicting the Hugoniot properties of several silicates [*Al'tshuler and Sharipdzhanov*, 1971]. It also produces reasonable bounds on the Hugoniot of a complex water-saturated grout [*Grady and Furnish*, 1988].

Hugoniot properties of water are from *Mitchell and Nellis* [1982] and the properties of MgO are from *Vassiliou and Ahrens* [1981]. Temperatures achieved upon shocking water are up to 3000 K hotter than those achieved along the brucite Hugoniot. MgO temperatures are up to 1500 K colder. To account for these differences, effective thermal expansion coefficients were computed at each pressure by comparing the Hugoniot density with that along a 300 K isotherm. The relevant isotherm data are from *Jackson and Niesler* [1982] and *Hemley et al.* [1987]. The volume change on melting for H_2O above 25 GPa was assumed to be 16.67 cm^3/g [*Zharkov and Trubitsyn*, 1978]. The thermal expansion coefficients were used to correct the densities to temperature conditions along the brucite Hugoniot. The resulting mixed oxide Hugoniot for brucite is shown as the dashed curve in Figure 2. Calculated densities along the mixed oxide Hugoniot are up to 4 % denser than the fit to the brucite data. Given the uncertainties in shock temperatures and the averaging procedure, the correspondence between these curves is reasonable. This implies that EOS data provide little additional information on the possible dehydration of brucite as reaction of (12) is predicted to have only a small effect on the EOS.

In summary, brucite shock data can be fit by a single EOS up to 97 GPa. Our preferred phase diagram is consistent with brucite dehydration occurring above 41 GPa. Brucite release data place a lower bound on dehydration at 26 GPa which is similar to the lower bound inferred from the room temperature compression curve of ice VII. There is no evidence for dehydration along the Hugoniot, possibly because of the small volume change associated with the reaction. Estimated mantle geotherms are shown in Figure 4. In normal mantle, brucite is not expected to be stable at pressures greater than a few GPa although it could persist to somewhat greater depths in slabs. Brucite is therefore unlikely to be a stable water-bearing phase in the lower mantle.

It is interesting to contrast brucite with the behavior of its isomorph, calcium hydroxide ($Ca(OH)_2$), which has been compressed statically to 38 GPa [*Meade and Jeanloz*, 1990]. Amorphization of $Ca(OH)_2$ was found to occur and this is interpreted as due to a phase transition below 11 GPa. Thus, magnesium hydroxide appears to be more stable than calcium hydroxide. This is analogous to the situation that occurs in oxides where magnesium oxide is more stable than calcium oxide.

Partial Release States

Partial release states for brucite are listed in Table 4 and shown in Figure 5. At intermediate pressures, most release points lie near or slightly to the left of the Hugoniot in accord with expected behavior. Near 10 GPa, the paths begin to diverge from the Hugoniot and final post shock densities are substantially less than the ambient density of brucite. This contrasts with release paths for silicates, including serpentine, which are anomalously steep due to phase changes [*Chhabildas and Miller*, 1985; *Tyburczy et al.*, 1991]. This reinforces the hypothesis that no large-volume phase change occurs over the pressure range of these experiments.

The rapid shallowing of the release paths is similar to the expected behavior of a material undergoing shock melting

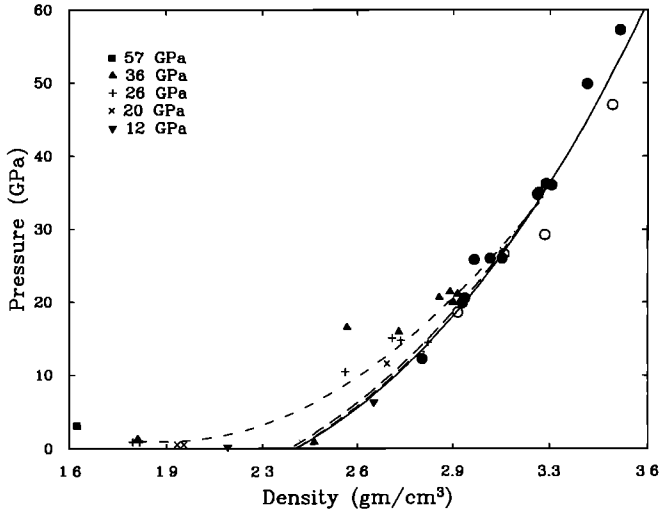

Fig. 5. Partial release states obtained for brucite. Hugoniot points are indicated by solid and open circles as in Figure 2. The solid curve is the fit to the data obtained in Figure 3. Other symbols represent measured partial release states; each symbol corresponds to a different peak Hugoniot pressure as indicated in the legend. Dashed curves are calculated Mie-Gruneisen release paths from Hugoniot pressures of 12 and 36 GPa. The dash-dot curve is the actual inferred release path from 36 GPa.

or vaporization upon adiabatic release [*Ahrens*, 1987]. Final postshock volume is generally a decreasing function of peak shock pressure, suggesting that increasing amounts of material are being volatilized upon release. Most of the decrease in postshock density occurs at pressures up to 26 GPa and there is relatively little reduction in postshock density after this. This agrees qualitatively with shock recovery data for brucite [*Lange and Ahrens*, 1984] in which it was found that brucite had lost 18% of its water at 13 GPa and 59% at 23 GPa.

We can attempt to quantify the amount of vaporization by comparing measured densities with those predicted by Mie-Gruneisen theory. Points on the release adiabat can be calculated from the Hugoniot state by combining the Mie-Gruneisen equation,

$$P = P_H + \frac{\gamma}{V}[E - E_H] \tag{17}$$

with the second law of thermodynamics under isentropic conditions,

$$dE = -PdV \tag{18}$$

to yield an incremental expression for the release paths [*McQueen et al.*, 1970; *Anderson et al.*, 1990]. Calculated release paths for selected Hugoniot pressures are shown in Figure 5 and Table 4.

Comparison of the calculated and measured release paths from 36 GPa shows that the actual release path is generally shallower than the Mie-Gruneisen prediction in which vaporization is not allowed to occur. At low pressures (~1 GPa), measured densities are generally much lower than expected from (17) and (18). The difference between the measured and calculated results can be used to infer the amount of material lost due to vaporization. In Figure 6, the density difference is attributed to water loss and plotted as a function of peak shock pressure. The agreement with shock recovery experiments [*Lange and Ahrens*, 1984] is quite good.

There is some evidence of heterogeneity in the release paths. Both shot 553 (36 GPa) and shot 199 (50 GPa) result in postshock densities that are large relative to the rest of the data set. This may be attributable to the heterogeneous nature of the shock deformation process and the important role played by thermal heterogeneities and local heat generation [*Grady*, 1980]. This type of behavior has been seen in the release data for a number of minerals [e.g., *Tyburczy et al.*, 1991].

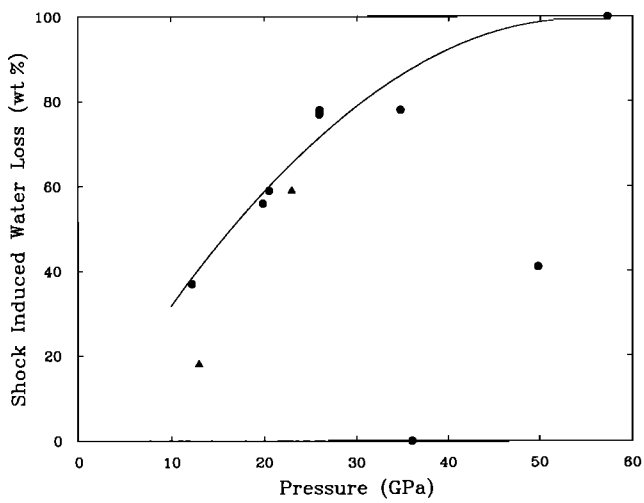

Fig. 6. Water loss upon isentropic release as a function of peak shock pressure. Water loss is inferred by comparing the measured final release density with calculated values based on Mie-Gruneisen theory. The circles are the data of this study, and the solid line is a fit to this data. The triangles are the results of solid recovery experiments [*Lange and Ahrens*, 1984].

The shock pressures expected to produce volatilization upon isentropic release can be estimated by the entropy method [*Ahrens and O'Keefe*, 1972]. In this technique, entropies achieved along the Hugoniot are compared to the entropy required to volatilize brucite at ambient pressures. If the release path is nearly isentropic, then the entropy should be largely unchanged as the release path passes through ambient pressure.

Temperatures required to dehydrate brucite have been measured by a number of workers [*Nutting*, 1943 ; *Ball and Taylor*, 1961; *Chen et al.*, 1989]. The dehydration of brucite is complex, involving the formation of an intermediate phase, and depends on the rate and duration of heating as well as grain size [*Ball and Taylor*, 1961]. The range of temperatures reported for the dehydration reaction is 475-750 K. Comparing the entropies at these temperatures [*Robie et al.*, 1978] with Hugoniot entropies indicates that brucite should dehydrate upon release from shock pressures between 27 and 49 GPa. The measured release paths as well as shock recovery data [*Lange and Ahrens*, 1984] both indicate that dehydration in brucite occurs at pressures as low as 12 GPa, considerably less than predicted theoretically.

Temperatures along the release path can be calculated from the following identity under isentropic conditions:

$$\frac{dT}{T} = -\gamma\frac{dV}{V} \tag{19}$$

The temperatures corresponding to the measured release points are listed in Table 4. It is interesting to note that final post-shock temperatures at and below 26 GPa are below the minimum temperature (475 K) needed to vaporize brucite under ambient conditions. Thus, post-shock temperatures are also a poor guide for predicting the onset of release vaporization. The intense heterogeneous deformation occurring during the shock process may play some role in facilitating volatilization, possibly by creating local thermal anomalies. Calculated temperatures and entropies may also be in error, particularly if our assumption about the Gruneisen parameter (equation (9)) does not hold.

Partial release states measured for brucite thus lend quantitative support to the results of earlier recovery experiments [*Lange and Ahrens*, 1984]. Brucite volatilizes upon release from pressures much lower than predicted theoretically, although the pressure required for complete volatilization is in agreement with the shock entropy prediction. This work, therefore, reinforces conclusions regarding the pressures and hence impact velocities required to partially and completely vaporize incoming material during the Earth's accretion [e.g., *Ahrens*, 1990]. While brucite is probably not an important source of volatiles in the incoming material, its structural and chemical simplicity make it an ideal material to test basic assumptions regarding the volatilization process.

Implications for the Earth's Interior

Recently, a number of dense high-pressure water bearing phases have been identified [*Ringwood and Major*, 1967; *Liu*,

1987; *Finger and Prewitt*, 1989; *Finger et al.*, 1989]. The possibility that these or other hydrous phases may play an important role in the Earth's lower mantle has not been considered previously. Brucite is not likely to be a lower mantle phase. However, the EOS data for $Mg(OH)_2$ obtained here, together with recent shock data for serpentine [*Tyburczy et al.*, 1991], can be used to estimate the effect of H_2O on seismic velocity and density profiles for the mantle.

Bulk sound velocities can be obtained from Hugoniot data by considering small isentropic expansions off the Hugoniot state and accounting for energy differences between the two curves using the Gruneisen parameter [*McQueen et al.*, 1967; *Ahrens*, 1987]:

$$V_\phi = \sqrt{\frac{K_s}{\rho}} = \left\{ \left(\frac{\partial P}{\partial \rho}\right)_H \left[1 - \left(\frac{1}{\rho_o} - \frac{1}{\rho}\right)\frac{\rho\gamma}{2}\right] + \frac{P\gamma}{2\rho} \right\}^{\frac{1}{2}} \tag{20}$$

Where V_ϕ is the bulk sound velocity and $\left(\frac{\partial P}{\partial \rho}\right)_H$ is the local slope of the Hugoniot. If the EOS can be represented in the form of (1), this becomes

$$V_\phi = \frac{c_o(1-\epsilon)}{(1-s\epsilon)^2}\left[1 + s\epsilon\left(1 - \frac{\gamma\epsilon}{1-\epsilon}\right)\right]^{\frac{1}{2}} \tag{21}$$

where the strain, ϵ, is given by

$$\epsilon = 1 - \frac{\rho_o}{\rho}. \tag{22}$$

Sound velocities calculated in this way are in good agreement with those measured by interferometric and optical analyzer techniques [*McQueen et al.*, 1984; *Chhabildas et al.*, 1988; *Duffy and Ahrens*, 1990*b*].

In Figure 7, bulk sound velocities are shown for brucite calculated from the equation of state and Gruneisen parameter determined above. Also shown are sound velocities for periclase, the anhydrous analogue of brucite, obtained from its EOS and Gruneisen parameter [*Vassiliou and Ahrens*, 1981]. The difference in sound speed between the two materials exhibits a marked reduction as a function of pressure. At pressures above 40 GPa, bulk sound velocities in MgO and $Mg(OH)_2$ overlap within their respective uncertainties. Similar results are obtained when serpentine is compared to its anhydrous analogues [*Tyburczy et al.*, 1991]. These results suggest that high-pressure hydrous phases or water-containing mixtures may be sufficiently compressed such that they are virtually indistinguishable from similar anhydrous assemblages in bulk sound velocity. The implication is that hydrous phases would not produce anomalous seismic velocities in the Earth.

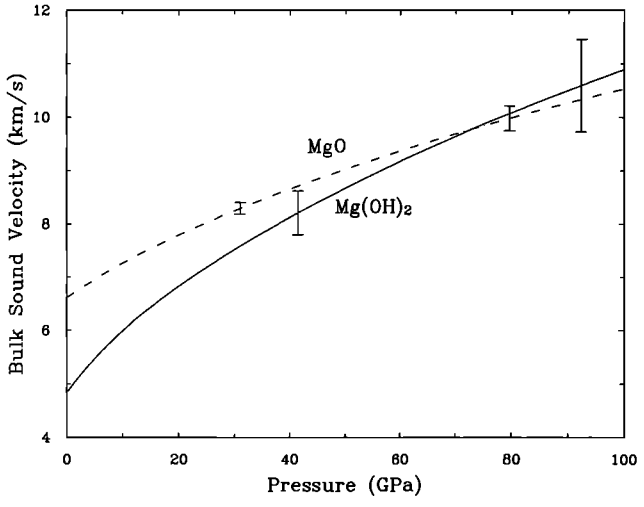

Fig. 7. Bulk sound velocity for brucite and periclase determined from their respective Hugoniots as discussed in the text. Brucite results are shown by the solid curve, and MgO results are the dash-dot curve. Representative error bars are shown at selected pressures.

The density of high-pressure water-bearing phases may also be addressed by the data obtained in this study. In Figure 8, pressure-density Hugoniot data for brucite (25-31 wt % H_2O) and serpentine (13-15 wt % H_2O) are compared to Hugoniot densities for some anhydrous phases at lower mantle pressures. It is evident that a considerable reduction in density occurs for assemblages containing substantial amounts of water.

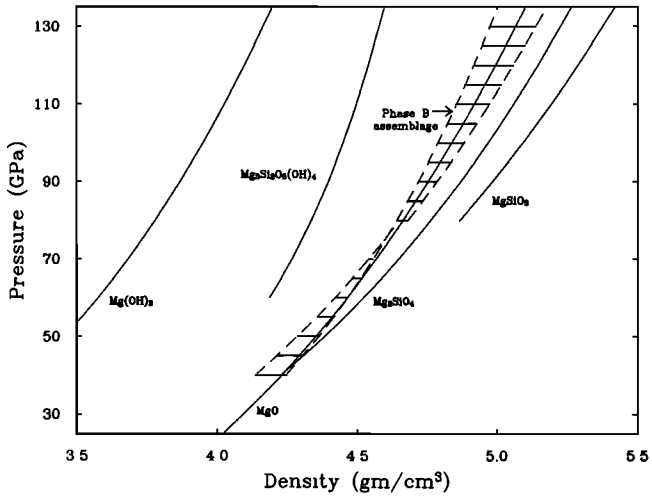

Fig. 8. Hugoniot data for both hydrous and anhydrous high-pressure phases that may be important in the lower mantle. The hatched region represents bounds for the predicted Hugoniot of the high-pressure assemblage of phase B composition.

The phase or phases that water would be found under lower mantle conditions is unknown. A wide variety of structures and chemistries are expected for hydrous magnesian silicates [*Finger and Prewitt*, 1989]. Two important structures under upper mantle conditions are phase A and phase B [*Ringwood and Major*, 1967]. A recent structure determination for phase B yielded the formula: $Mg_{12}Si_4O_{19}(OH)_2$ with Si in both octahedral and tetrahedral coordination [*Finger et al.*, 1989]. The stability of phase B has been demonstrated to 20 GPa and 1000°C [*Liu*, 1986]. At higher pressures, it is reasonable to suppose that phase B would transform to one or more phases involving complete octahedral coordination of silicon. A theoretical Hugoniot for this high-pressure assemblage can be constructed by considering the following hypothetical reactions:

$$Mg_{12}Si_4O_{19}(OH)_2 \rightleftharpoons 4Mg_2SiO_4 + 3MgO + Mg(OH)_2$$

$$Mg_{12}Si_4O_{19}(OH)_2 \rightleftharpoons 4MgSiO_3 + 7MgO + Mg(OH)_2$$

$$Mg_{12}Si_4O_{19}(OH)_2 \rightleftharpoons 4SiO_2 + 11MgO + Mg(OH)_2$$

Theoretical Hugoniots were constructed using the weight

fraction additivity scheme discussed above without correcting for temperature differences. The sources for high pressure Hugoniot data for silicates and oxides are: MgO [*Vassiliou and Ahrens*, 1981]; SiO_2 [*Lyzenga and Ahrens*, 1983]; $MgSiO_3$ [*Simakov and Trunin*, 1973]; Mg_2SiO_4 [*Jackson and Ahrens*, 1979].

Calculated densities for the phase B assemblage closely parallel densities for MgO throughout the lower mantle pressure range (Figure 8). At 100 GPa, the density of phase B is within 1% of MgO and is about 3% less dense than the Mg_2SiO_4 high-pressure phase and 5% less dense than the $MgSiO_3$ high-pressure phase. The near equivalence in density of phase B to that of MgO suggests that in the upper mantle, the amount of water present is limited, in principle, only by the quantity of phase B present. The possible presence of water in the lower mantle is further discussed below.

EOS data for brucite can be used to constrain the range of possible water content of the lower mantle. In Figure 9, the Hugoniot for En_{85} ($(Mg_{.85}Fe_{.15})SiO_3$) [*Trunin et al.*, 1965] is shown along with a calculated Hugoniot for brucite with 0.15 mole fraction Fe, Br_{85} ($(Mg_{.85}Fe_{.15})(OH)_2$). The Br_{85} Hugoniot was calculated by mixing the Hugoniots of MgO, H_2O, and FeO [*Jeanloz and Ahrens*, 1980]. The ability of the brucite structure to accommodate iron is enhanced markedly by the application of pressure. Fe concentrations of 21 atomic % have been achieved at 3 kbar [*Delnavaz and Allmann*, 1988]. Natural samples with about 10 mol. % Fe have been reported [*Berman*, 1932]. Temperatures along the Hugoniot are much hotter (3000-5000 K) at lower mantle pressures than corresponding geotherms (2000-3000 K). We assume a maximal density correction of 0.10 g/cm^3 for both En_{85} and Br_{85} [*Watt and Ahrens*, 1986]. By choosing a maximal temperature correction and a relatively high iron concentration, we are able to estimate the maximum amount of H_2O that would be consistent with seismic density profiles. The pressure-density curves in Figure 9 are corrected to geotherm temperatures. Also shown is Earth model PREM [*Dziewonski and Anderson*, 1981] with 0.5% uncertainty. En_{85} alone matches PREM within its uncertainty. PREM can also be fit by averaging in successively greater fractions of Br_{85} up to 10 wt % as shown in the figure. Larger amounts of Br_{85} are allowed only if compensated by some additional high-density material. The maximum fraction of brucite corresponds to 3 wt. % H_2O. Thus, seismic density profiles and shock data for enstatite and brucite constrain the water content of the lower mantle to be 0-3 wt. %. This conclusion is unlikely to change significantly no matter what the stable H_2O-bearing phase is under lower mantle conditions as long as the mixing model discussed above holds. Denser water-bearing phases may be present in greater quantities but the total amount of water allowed must remain nearly fixed. The applicability of the mixed oxides model for H_2O-bearing phases has been confirmed by *Tyburczy et al.* [1991] who demonstrated that the high-pressure phase of serpentine can be modeled using the Hugoniots of $Mg(OH)_2$, MgO, and SiO_2.

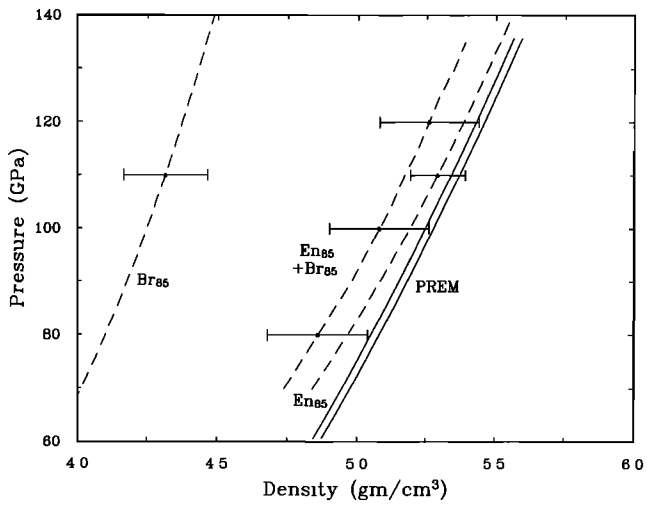

Fig. 9. Hugoniot data for enstatite and brucite compared with Earth model PREM (solid curves). The curve labeled Br_{85} represents the brucite Hugoniot adjusted to geotherm temperatures and containing 0.15 mole fraction Fe. The curve labeled En_{85} is the Hugoniot for enstatite also with 0.15 mole fraction iron and corrected to geotherm temperatures. The curve En_{85} + Br_{85} represents enstatite mixed with 10 % brucite by weight. This is the maximum amount of brucite that can be mixed with enstatite and still agree with the seismic model PREM within respective uncertainties. Representative error bars are included at selected pressures.

A lower mantle water content of 3 wt. % would correspond to 8.8 x 10^{25} g of water. The Earth's oceans contain approximately 1.4 x 10^{24} g of water [*Walker*, 1977] meaning that the lower mantle could contain between 0-63 oceans' worth of water. Petrological estimates suggest the mantle contains 0.1 wt. % H_2O [*Ringwood*, 1975]. Estimates based on accretion scenarios have concluded that greater than five times [*Liu*, 1987], or 3-10 times [*Abe and Matsui*, 1986] the mass of the oceans are contained in the mantle. Thus, the amount of water required in accretion and petrological models can easily be accommodated by seismic density profiles.

The existence of high-pressure water-bearing minerals has implications for the accretion of the Earth and the evolution of the atmosphere. A consideration of present accretion models allows the possible role of hydrous minerals to be better understood. *Ringwood* [1979] identifies two stages in the accretion process: mode A and mode B. During mode A, incoming planetesimals are not completely devolatilized. This phase continues until the Earth reaches 0.2-0.5 times its present radius [*Ahrens*, 1990]. Assuming an average density of 5.5 g/cm^3, 7.5 x 10^{26} g is the maximum amount of material that could have accreted during this phase. Assuming all volatiles are incorporated into the Earth, then 3 wt. % H_2O could result if the accreting planetesimals averaged 12 wt. % H_2O. While this is typical of C1 (20 wt. % H_2O) and C2 (13 wt. % H_2O) meteorites [*Mason*, 1971], it is considerably greater than previous estimates of planetesimal H_2O contents (0.1-3.0 wt. % H_2O) [*Ringwood*, 1979; *Liu*, 1987].

During mode B, incoming material is completely volatilized and a number of processes are occurring which might affect the incorporation of water into the interior. The rehydration of anhydrous silicates in the planet's regolith is one such process. It is especially important in the absence of an atmosphere [*Zahnle et al.*, 1988]. If this process is very efficient, large amounts of water may still be incorporated into the interior at large planetary radii [*Jakosky and Ahrens*, 1979]. As a steam atmosphere builds through impact devolatilization, surface temperatures may rise until a magma ocean forms [*Abe and Matsui*, 1986; *Zahnle et al.*, 1988]. Large amounts of volatiles can be dissolved in silicate melts. These volatiles may then be transferred into the interior convectively and could be retained when the magma ocean freezes at high pressure [*Liu*, 1987].

Atmospheric escape of H_2 and impact erosion of the atmosphere also affect the volatile budget of the planet. Recent models suggest that in most scenarios these processes are not highly efficient in reducing a planet's total volatile budget [*Zahnle et al.*, 1988; *Chyba*, 1990]. Nonetheless, there is insufficient evidence to fully evaluate the importance of these processes. Large impacts at late times can have a large effect on the accretion process. A Mars-sized bolide could strip away the primitive atmosphere and extensively melt the mantle of the impacted planet. In this scenario, the stability of high-pressure water-bearing phases is of great importance as the present atmosphere might be formed by subsequent degassing of the mantle. The existence of a deep water reservoir that survives the bolide impact may provide a source for the atmosphere.

In the models of *Abe and Matsui* [1986], the total mass of water in the atmosphere is independent of the water content of the planetesimals. Any excess water is buried in the mantle (3-10 oceans' worth in their models). The question remains whether this water could remain buried in the mantle throughout the lifetime of the Earth. The existence of high-pressure water-bearing phases such as phase B suggests that water can be retained, at least under upper mantle conditions. The problem also hinges on the relative efficiency of volatile release at the ridges versus regassing at the trenches. The details of the convective system are also important.

In summary, the present data provide support for the two stage accretion model in which some fraction of incoming volatiles can be retained in the growing planet. For brucite, impact-induced volatilization begins at 12 GPa and is complete near 56 GPa. EOS data for brucite do not preclude the continued existence of a large water reservoir in the Earth's interior. However, brucite itself is probably not stable in most of the mantle.

SUMMARY

1. New shock equation of state data on magnesium hydroxide between 12 and 60 GPa are reported. The present data are slightly more incompressible than the data of *Simakov et al.* [1974]. Taken together, brucite data up to 97 GPa can be fit by a single U_s-u_p relation: $U_s = 4.76 + 1.35u_p$. Third-order Birch-Murnaghan parameters are $K_{os} = 51 \pm 4$ GPa and $K'_{os} = 5.0 \pm 0.4$.

2. While a single EOS satisfies all brucite data, brucite may dehydrate at high pressure. A lower bound for this dehydration reaction is inferred from release data to be 26 GPa. EOS data for brucite were combined with thermodynamic data to assess the stability of brucite at high pressure and temperature. The equilibrium boundary for dehydration along the Hugoniot is inferred to be near 41 GPa. Calculated phase boundaries are consistent with experimental data. The measured EOS of brucite is similar to that predicted for the mixture MgO + H_2O.

3. Brucite volatilizes upon release from shock pressures as low at 12 GPa and volatilization is nearly complete upon release from 56 GPa, in good agreement with shock recovery data. The shock entropy method overestimates the pressures required to initiate volatilization in this material.

4. While brucite is unlikely to be stable in the lower mantle, brucite EOS data can be used to evaluate the effect of H_2O on lower mantle properties through the use of mixing models. Bulk sound velocities calculated for $Mg(OH)_2$ are indistinguishable from MgO at pressures above 40 GPa. The presence of hydrous assemblages in the lower mantle may not, therefore, produce a seismic bulk velocity discontinuity. Data on brucite and other high-pressure phases were compared to seismic density profiles. The H_2O content of the lower mantle is constrained to be 0-3 wt. %.

Acknowledgments. We appreciate the careful construction and execution of these experiments by Michael Long and Papo Gelle. We thank James Tyburczy, John Brodholt, Toshimori Sekine, Lawrence Finger, and an anonymous reviewer for valuable comments and discussion. The research was supported by NSF and NASA grants. Division of Geological and Planetary Sciences, California Institute of Technology contribution 4909.

REFERENCES

Abe, Y., and T. Matsui, Early evolution of the Earth: Accretion, atmosphere formation and thermal history, *Proc. Lunar Planet. Sci. Conf. 17th, Part 1, J. Geophys. Res., 91, suppl.*, E291-E302, 1986.

Ahrens, T. J., Shock wave techniques for geophysics and planetary physics, in *Methods of Experimental Physics*, vol. 24, edited by C. G. Sammis and T. L. Henyey, pp. 185-235, Academic, San Diego, Calif., 1987.

Ahrens, T. J., Earth accretion, in *Origin of the Earth*, edited by J. Jones and H. Newson, pp. 211-227, Oxford University Press, New York, 1990.

Ahrens, T. J., and R. Jeanloz, Pyrite: shock compression, isentropic release, and composition of the Earth's core, *J. Geophys. Res, 92*, 10,363-10,375, 1987.

Ahrens, T. J., and J. D. O'Keefe, Shock melting and vaporization of lunar rocks and minerals, *Moon, 4*, 214-249, 1972.

Al'tshuler, L. V., and I. I. Sharipdzhanov, Additive equations of state of silicates at high pressure, *Izv. Earth Phys., 3*, 11-28, 1971.

Anderson, C. E., T. G. Trucano, and S. A. Mullin, Debris cloud dynamics, *Int. J. Impact Eng., 9*, 89-113, 1990.

Ball, M. C., and H. F. W. Taylor, The dehydration of brucite, *Min. Mag., 32*, 754-766, 1961.

Berman, H., Fibrous brucite from Quebec (with a note on its structure after dehydration by C. D. West), *Am. Mineral., 17*, 313-316, 1932.

Birch, F., Finite strain isotherm and velocities for single-crystal and polycrystalline NaCl at high pressures and 300 K, *J. Geophys. Res., 83*, 1257-1268, 1978.

Canil, D., and C. M. Scarfe, Phase relations in peridotite+CO_2 systems to 12 GPa: implications for the origin of kimberlite and carbonate stability in the Earth's upper mantle, *J. Geophys. Res., 95*, 15,805-15,816, 1990.

Chen, I., S. Hwang, and S. Chen, Chemical kinetics and reaction mechanism of thermal decomposition of aluminum hydroxide and magnesium hydroxide at high temperatures (973-1123 K), *Ind. Eng. Chem. Res., 28*, 738-742, 1989.

Chhabildas, L. C., and J. M. Miller, Release-adiabat measurements in crystalline quartz, Sandia Natl. Lab., *Rep. SAND85-1092*, Albuquerque, N. M., 1985.

Chhabildas, L. C., J. R. Asay, and L. M. Barker, Shear strength of tungsten under shock- and quasi-isentropic loading to 250 GPa, Sandia Natl. Lab., *Rep. SAND88-0306*, Albuquerque, N. M., 1988.

Chyba, C. F., Impact delivery and erosion of planetary oceans in the early inner solar system, *Nature, 343*, 129-133, 1990.

Delnavaz, H., and R. Allmann, Synthesis of Fe-brucite, coalingite, and pyroaurite in system MgO – Fe – O_2 – H_2O – (CO_2), *Z. Kristallogr., 183*, 175-178, 1988.

Duffy, T. S., and T. J. Ahrens, New evidence for lower mantle hydrous phases (abstract), *Eos, Trans. AGU, 71*, 528, 1990*a*.

Duffy, T. S., and T. J. Ahrens, Sound velocity measurements at high temperature and pressure in metals and minerals through shock loading (abstract), *Eos, Trans. AGU, 71*, 619, 1990*b*.

Dziewonski, A. D., and D. L. Anderson, Preliminary reference Earth model, *Phys. Earth Planet. Inter., 25*, 297-356, 1981.

Finger, L. W., and C. T. Prewitt, Predicted compositions for high-density hydrous magnesium silicates, *Geophys. Res. Lett., 16*, 1395-1397, 1989.

Finger, L. W., J. Ko, R. M. Hazen, T. Gasparik, R. J. Hemley,

C. T. Prewitt, and D. J. Weidner, Crystal chemistry of phase B and an anhydrous analogue: Implications for water storage in the upper mantle, *Nature, 341,* 140-142, 1989.

Grady, D. E., Shock deformation of brittle solids, *J. Geophys. Res., 85,* 913-924, 1980.

Grady, D. E., and M. D. Furnish, Shock- and release-wave properties of MJ-2 grout, Sandia Natl. Lab., *Rep. SAND88-1642,* Albuquerque, N. M., 1988.

Halbach, H., and N. D. Chatterjee, An empirical Redlich-Kwong-type equation of state for water to 1000 °C and 200 Kbar, *Contrib. Mineral. Petrol., 79,* 337-345, 1982.

Heinz, D. L., and R. Jeanloz, The equation of state of the gold calibration standard, *J. Appl. Phys., 55,* 885-893, 1984.

Hemley, R. J., A. P. Jephcoat, H. K. Mao, C. S. Zha, L. W. Finger, and D. E. Cox, Static compression of H_2O-ice to 128 GPa (1.28 Mbar), *Nature, 330,* 737-740, 1987.

Hurlbutt, C. S., and C. Klein, *Manual of Mineralogy,* 532 pp., John Wiley, New York, 1977.

Irving, A. J., W.-L. Huang, and P. J. Wyllie, Phase relations of portlandite, $Ca(OH)_2$ and brucite $Mg(OH)_2$ to 33 kilobars, *Am. J. Sci., 277,* 313-321, 1977.

Jackson, I., and T. J. Ahrens, Shock wave compression of single-crystal forsterite, *J. Geophys. Res., 84,* 3029-3048, 1979.

Jackson, I., and H. Niesler, The elasticity of periclase to 3 GPa and some geophysical implications, in *High Pressure Research in Geophysics,* edited by S. Akimoto and M. H. Manghnani, pp. 93-133, Center for Academic Publishing, Tokyo, 1982.

Jakosky, B. M., and T. J. Ahrens, The history of an atmosphere of impact origin, *Proc. Lunar Planet. Sci. Conf., 10th,* 2727-2739, 1979.

Jeanloz, R., Shock-wave equation of state and finite strain theory, *J. Geophys. Res., 94,* 5873-5886, 1989.

Jeanloz, R., and T. J. Ahrens, Equations of state of FeO and CaO, *Geophys. J. R. Astron. Soc., 62,* 505-528, 1980.

Kanzaki, M., Thermal analysis in a multi-anvil high-P apparatus (abstract), *Eos, Trans. AGU, 71,* 1697, 1990.

Kruger, M. B., Q. Williams, and R. Jeanloz, Vibrational spectra of $Mg(OH)_2$ and $Ca(OH)_2$ under pressure, *J. Chem. Phys., 91,* 5910-5915, 1989.

Lange, M. A., and T. J. Ahrens, FeO and H_2O and the homogeneous accretion of the Earth, *Earth Planet. Sci. Lett., 71,* 111-119, 1984.

Liu, L., Phase transformations in serpentine at high pressures and temperatures and implications for subducting lithosphere, *Phys. Earth Planet. Inter., 42,* 255-262, 1986.

Liu, L., Effect of H_2O on the phase behavior of the forsterite-enstatite system at high pressures and temperatures and implications for the Earth, *Phys. Earth Planet. Inter., 49,* 142-167, 1987.

Liu, L., Water, low-velocity zone and the descending lithosphere, *Tectonophysics, 164,* 41-48, 1989.

Lyzenga, G. A., and T. J. Ahrens, The relation between the shock-induced free-surface velocity and the postshock specific volume of solids, *J. Appl. Phys., 49,* 201-204, 1978.

Lyzenga, G. A., and T. J. Ahrens, Shock temperatures of SiO_2 and their geophysical implications, *J. Geophys. Res., 88,* 2431-2444, 1983.

Marsh, S. P., *LASL Shock Hugoniot Data,* 658 pp., University of California Press, Berkeley, 1980.

Mason, B., *Handbook of Elemental Abundances in Meteorites,* 555 pp., Gordon and Breach, New York, 1971.

McGovern, P. J., and G. Schubert, Thermal evolution of the Earth: effects of volatile exchange between atmosphere and interior, *Earth Planet. Sci. Lett., 96,* 27-37, 1989.

McQueen, R. G., S. P. Marsh, and J. N. Fritz, Hugoniot equation of state of twelve rocks, *J. Geophys. Res., 72,* 4999-5035, 1967.

McQueen, R. G., S. P. Marsh, J. W. Taylor, J. N. Fritz, and W. J. Carter, The equation of state of solids from shock wave studies, in *High-Velocity Impact Phenomena,* edited by R. Kinslow, pp. 294-419, Academic, San Diego, Calif., 1970.

McQueen, R. G., J. N. Fritz, and C. E. Morris, The velocity of sound behind strong shock waves in 2024 Al, in *Shock Waves in Condensed Matter - 1983,* edited by J. R. Asay, R. A. Graham, and G. K. Straub, pp. 95-98, Elsevier, New York, 1984.

Meade, C., and R. Jeanloz, Acoustic emission from serpentine at high pressures and low temperatures: Implications for the origin of deep-focus earthquakes (abstract), *Eos, Trans. AGU, 70,* 1321, 1989.

Meade, C., and R. Jeanloz, Static compression of $Ca(OH)_2$ at room temperature: observations of amorphization and equation of state measurements to 10.7 GPa, *Geophys. Res. Lett., 17,* 1157-1160, 1990.

Mishima, O., and S. Endo, Melting curve of Ice VII, *J. Chem. Phys., 68,* 4417-4418, 1978.

Mitchell, A. C., and W. J. Nellis, Equation of state and electrical conductivity of water and ammonia shocked to the 100 GPa (1 Mbar) pressure range, *J. Chem Phys., 76,* 6273-6281, 1982.

Nutting, P., Some standard thermal dehydration curves for minerals, *U.S. Geol. Surv., Prof. Pap. 197-E,* 197-216, 1943.

Ringwood, A. E., *Composition and Petrology of the Earth's Mantle* , 618 pp., McGraw-Hill, New York, 1975.

Ringwood, A. E., *Origin of the Earth and Moon,* 295 pp., Springer, New York, 1979.

Ringwood, A. E., and A. Major, High-pressure reconnaissance investigations in the system $Mg_2SiO_4 - MgO - H_2O$, *Earth Planet. Sci. Lett., 2,* 130-133, 1967.

Roberts, W. L., T. J. Campbell, and G. R. Rapp, *Encyclopedia of Minerals,* 2nd ed., 979 pp., Van Nostrand Reinhold, New York, 1990.

Robie, R. A., B. S. Hemingway, and J. R. Fischer, Thermodynamic properties of minerals and related substances at 298.15 K and 1 bar (10^5 Pascals) pressure and at higher temperatures, *U.S. Geol. Surv. Bull., 1452,* 456 pp., 1978.

Saxena, S. K., Assessment of bulk modulus, thermal expansion and heat capacity of minerals, *Geochim. Cosmochim. Acta, 53,* 785-789, 1989.

Saxena, S. K. and Y. Fei, High pressure and temperature fluid fugacities, *Geochim. Cosmochim. Acta, 51,* 783-791, 1987.

Schramke, J. A., D. M. Kerrick, and J. G. Blencoe, Experimental determination of the brucite = periclase + water equilibrium with a new volumetric technique, *Am. Mineral., 67,* 269-276, 1982.

Simakov, G. V., and R. F. Trunin, On the existence of the overdense perovskite structures in magnesian silicates under conditions of high pressure, *Izv. Earth Phys., 9,* 603-604, 1973.

Simakov, G. V., M. N. Pavlovsky, N. G. Kalashnikov, and R. F. Trunin, Shock compressibility of twelve minerals, *Izv. Earth Phys., 10,* 11-17, 1974.

Skinner, B. J., Thermal expansion, in *Handbook of Physical Constants,* edited by S. P. Clark, pp. 75-96, Geological Society of America, New York, 1966.

Suzuki, I., Thermal expansion of periclase and olivine and their anharmonic properties, *J. Phys. Earth, 23,* 145-159, 1975.

Trunin, R. F., V. I. Gon'shakova, G. V. Simakov, and N. E. Galdin, A study of rocks under the high pressures and temperatures created by shock compression, *Izv. Earth Phys.,* no. *8,* 579-586, 1965.

Tyburczy, J. A., T. S. Duffy, T. J. Ahrens, and M. A. Lange, Shock wave equation of state of serpentine to 150 GPa: Implications for the occurrence of water in the Earth's lower mantle, in press, *J. Geophys. Res.,* 1991.

Vassiliou, M. S., and T. J. Ahrens, Hugoniot equation of state of periclase to 200 GPa, *Geophys. Res. Lett., 8,* 229-232, 1981.

Walker, J. C. G., *Evolution of the Atmosphere,* 318 pp., MacMillan, New York, 1977.

Watt, J. P., and T. J. Ahrens, Shock wave equation of state of enstatite, *J. Geophys. Res., 91,* 7495-7503, 1986.

Yamaoka, S., O. Fukunaga, and S. Saito, Phase equilibria in the system $MgO-H_2O$ at high temperatures and very high pressures, *J. Am. Ceram. Soc., 53,* 179-181, 1970.

Zahnle, K. J., J. F. Kasting, and J. B. Pollack, Evolution of a steam atmosphere during Earth's accretion, *Icarus, 74,* 62-97, 1988.

Zharkov, V. N., and V. P. Trubitsyn, *Physics of Planetary Interiors,* 388 pp., Pachart, Tucson, Ariz., 1978.

T. J. Ahrens and T. S. Duffy, Seismological Laboratory, California Institute of Technology, Pasadena, CA 91125.

M. A. Lange, Alfred Wegner Institute for Polar and Marine Research, Bremerhaven, Germany.

(Received August 13, 1990;
revised March 5, 1991;
accepted April 3, 1991.)